Electric Power Systems Research 245 (2025) 111601

Contents lists available at ScienceDirect

Electric Power Systems Research

journal homepage: www.elsevier.com/locate/epsr

AI-driven single-end partial discharge localization in power cables based on time domain reflectometry and transfer function analyses

Morteza Shamsoddini [a], Tongkun Lan [a], Seokbum Ko [a,*], Chi Yung Chung [b]

[a] Department of Electrical and Computer Engineering, University of Saskatchewan, Saskatoon, SK, Canada
[b] Department of Electrical and Electronic Engineering, Hong Kong Polytechnic University, Saskatoon, Hong Kong, China

ARTICLE INFO

Keywords:
Attenuation
Cable
Deep learning
Partial discharge
Transfer function
Traveling wave

ABSTRACT

Accurate localization of partial discharge (PD) in power cables is critical for minimizing downtime and associated costs. Therefore, this paper presents a single-end localization method that simplifies implementation by avoiding the complexities of double-sided or distributed schemes. A fundamental challenge for online monitoring systems based on a single-end measurement scheme is the accurate and autonomous identification of incident pulses and their corresponding reflections, particularly in environments where impulse noise and PD-like interference are present and may resemble actual PD pulses, making it difficult to distinguish true events from interfering pulses. In this regard, this paper proposes a method based on the traveling wave characteristics and transfer function (TF) analysis to pinpoint the PD source accurately, even in challenging conditions such as multi-path propagation, impulse noise, and simultaneous PD events. To achieve this, a cable-specific attenuation characteristic is developed and incorporated within a two-step signal segmentation algorithm, and then the U-Net model is employed to estimate PD pulses' arrival time precisely. Additionally, the proposed method provides a statistical analysis of its maximum localization capability based on the noise level and cable length. The performance of the method is assessed under both homogeneous and inhomogeneous cable configurations. The results demonstrate a localization error of less than 1% for a 1.5 km cable.

1. Introduction

Failure of insulation in power cables in distribution and transmission networks can lead to a cascade of effects, including faults, energy supply disruptions, and blackouts, all of which can have social and economic consequences. Insulation failure is responsible for over 85% of failures in power systems [1]. One of the primary factors contributing to the degradation of cable insulation is the occurrence of partial discharge (PD) events. These events typically arise from imperfections, voids, or discontinuities present in the cable's insulation [2].

When PD occurs within the cable insulation, it progressively degrades the insulation over time and, if left unresolved, can ultimately lead to complete insulation breakdown. To mitigate the impact of PD and decelerate insulation degradation, nanocomposite technologies have been developed and applied recently to enhance dielectric strength and reduce PD currents, extending the operational lifespan of power cables [3–5]. Despite these advancements, assessing the condition of power cables throughout their service life continues to hold significant importance. Monitoring PD activities is an effective method for assessing the condition of power cables, acquiring insights into cable insulation health, and identifying potential future failures [6–8]. Implementing online monitoring systems to assess cable conditions by tracking PD activity not only enables the analysis of PD progression trends but also assists transmission and distribution facility owners in planning maintenance activities effectively and helps minimize the risk of unscheduled supply interruptions. In this regard, accurate localization of PD events and timely remedial actions are essential for effective maintenance, ultimately reducing both maintenance time and costs.

Numerous researchers have proposed various PD localization methods to address the need for accurate localization. Among these, time-domain reflectometry (TDR) is the most widely adopted approach for online PD localization [9–15]. This method is based on the traveling wave theory. In fact, when a PD event initiates, it generates electromagnetic waves that propagate toward the cable ends, and the objective of the TDR approach is to determine the arrival times of these waves, as this information is required for locating the PD source. Based on the number of measurement devices and their coordination schemes, TDR methods are typically classified into three main categories: single-terminal [9–11], double-sided [12,13], and multi-terminal [14,15].

In the single-end measurement scheme, the arrival times of incident and reflected PD pulses are determined using a single measurement

* Corresponding author.
E-mail address: seokbum.ko@usask.ca (S. Ko).

https://doi.org/10.1016/j.epsr.2025.111601
Received 31 December 2024; Received in revised form 26 February 2025; Accepted 5 March 2025
Available online 17 March 2025

device positioned at one end of the cable [16]. Various techniques, including trigger levels, signal energy analysis, and the Akaike information criterion have been developed to estimate the arrival times of traveling waves generated by PD events [17–19]. However, single-end methods have two significant drawbacks that affect their accuracy. The first drawback is the frequency-dependent nature of wave velocity, which has been further investigated in [10,16,20]. The authors in [10] proposed an improved single-end method based on iterative propagation velocity adjustment using the location and propagation time estimation. This method measures the arrival times of PD pulses to calculate an initial location, and subsequently refines the results by accounting for wave velocity variations through an iterative approach. Also, in [20] the frequency-dependent nature of the phase velocity is considered, and this velocity is applied to correct the phase difference of the PD signals. However, the precision of these methods can be impacted by factors such as the sampling rate and the cable length.

The second drawback of single-end methods is their dependence on the arrival time of the reflected pulse. Due to the longer propagation distance, the reflected pulse experiences greater attenuation and dispersion, challenging its detection and precise arrival time estimation. To address this issue, the double-sided and multi-end methods have been proposed. The double-sided scheme utilizes two synchronized measurement devices at both ends of the cable, to detect the arrival time of the incident pulse. While this technique addresses the dependence on reflection pulses and enhances localization accuracy, its performance is susceptible to inaccuracies in time synchronization between devices, variations in pulse propagation velocity, and noise interference.

Recent studies have introduced time synchronization techniques based on signal injection [12] and linear frequency modulation [13], which improve timing discrepancies and mitigate propagation velocity variations. Despite these improvements, implementing double-sided schemes remains complex and costly. Consequently, multi-end schemes based on distributed sensing structures have recently attracted researchers' attention [14,15]. This scheme employs multiple devices placed at various points along the cable, eliminating the need for time synchronization. This scheme leverages distributed optical fiber sensing technology for detecting cable PDs. Phase-sensitive optical time-domain reflectometry (ϕ-OTDR) [21] and coherent optical time-domain reflectometry (COTDR) [14] are two main approaches within this domain. Despite their capabilities, these methods suffer drawbacks, such as difficulties in installing the sensing array over large areas, high implementation costs, and the computational complexity associated with processing large volumes of data.

Building on the need to address the limitations of TDR methods and reduce the complexity associated with estimating signal arrival times and practical implementation, alternative techniques such as frequency domain reflectometry (FDR) have been proposed [11,22]. In the FDR method, a frequency sweep signal containing a wide range of high-frequency components is injected into the cable under test, enabling fault location identification by analyzing the different parameters such as broadband impedance spectroscopy (BIS) [22]. Also, this field's particular line of studies focuses on transfer function (TF) identification. TF identification is grounded in the high-frequency modeling of power cables [23], establishing a correlation between PD events' location and mathematical or experimental relationships derived from system analysis. These relationships are developed by examining the impact of the cable and associated components' TF on the propagation of PD pulses along the cable, culminating in a method for PD localization.

One group of TF-based approaches is founded on theoretical formulations [24–27]. In these methods, the parameters of the cable and other system components are analyzed to derive a mathematical relationship between the cable's TF and the distance traveled by the PD pulse. Another group of approaches involves the experimental determination of the cable's TF. In these approaches, the cable is taken offline, a signal is injected at one end, and measurements are collected at various locations along the cable, which enables the development of an empirical relation correlating the measured TF to the PD pulse's propagation distance [28,29]. Experimental methods typically provide higher precision but necessitate taking the cable out of service to measure the TF. In contrast, theoretical methods rely on the cable's geometric and electrical parameters, thus avoiding service interruptions.

While TDR and FDR approaches have yielded significant insights, recent advancements in artificial intelligence (AI) offer new opportunities for PD source localization. Although AI techniques have been extensively utilized in PD identification, their application to PD source localization in power cables remains comparatively underexplored. For instance, [30] introduced a deep learning (DL)-based localization method that relies on DL models to determine signal arrival times. This approach analyzes the localization challenge as a computer science issue, which may lead to overlooking useful insights derived from established localization methodologies. Consequently, a research gap remains in developing approaches that synergistically combine AI capabilities with mainstream localization approaches to achieve superior accuracy and performance.

Various methodologies, as discussed, have been developed to address the challenges of arrival time estimation, attenuation, and dispersion in power cables for PD localization. With the growing capabilities and widespread adoption of DL models in different fields, there is significant potential to leverage these tools to enhance single-end localization methods. This approach helps to avoid the complexities and high costs caused by synchronized-based systems, distributed sensing technologies, and injection-based methods, providing a straightforward, economically viable solution that is still accurate for online monitoring systems. However, single-end localization methods face critical limitations that need further investigation. No prior studies have explored how such systems can identify relevant incident and reflection pulses, specifically in environments with multi-path propagation, impulse noise, or simultaneous PD events. Additionally, the operational capabilities of single-end localization methods, such as their effectiveness concerning maximum signal-to-noise ratio (SNR) levels and the cable lengths they can reliably monitor, have yet to be systematically examined.

To cover the identified gaps, this paper proposes an online single-end PD localization framework for power cables that integrates DL capabilities with insights from TDR and TF analyses. The proposed approach introduces a cable-specific attenuation characteristic to effectively identify relevant incident and reflection pulses, even under challenging conditions such as impulse noise, multi-propagation path, and simultaneous PD events. The derived attenuation characteristic is then employed within a two-step signal partitioning algorithm. The first level identifies segments with characteristics resembling PD pulses based on correlation calculations. In the second level, the cable-specific attenuation characteristic, derived from the TF analysis, is used to distinguish relevant incident and reflection pulses among the set of separated pulses. Finally, to address the time estimation challenge and enhance accuracy without additional components, U-Net, a DL-based model, is employed to determine the precise arrival times of the pulses.

The remainder of this paper is structured as follows: Section 2 presents the development of cable attenuation characteristics, based on the theoretical foundations of traveling wave theory and TF analysis. Section 3 describes the localization methodology and the interaction of its components in detail. The feasibility and effectiveness of the proposed method are then evaluated under various scenarios in Section 4. Finally, Section 5 provides the conclusions.

2. Theoretical background

This section explores the theoretical foundations by examining the relationship between traveling wave theory, the core principle behind TDR, and TF analysis, which is derived from FDR methodologies. Building on these fundamental concepts, the cable-specific attenuation characteristic is then developed.

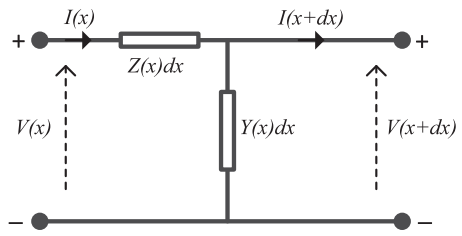

Fig. 1. A typical cable model.

2.1. Cable model

A typical power cable can be modeled like a transmission line, as illustrated in Fig. 1. In this model, the relationship between the input and output currents and voltages in the frequency domain, with respect to an infinitesimal segment dx, is given by:

$$\frac{\partial}{\partial x}\begin{bmatrix} V(x,\omega) \\ I(x,\omega) \end{bmatrix} = \begin{bmatrix} 0 & Z(\omega) \\ Y(\omega) & 0 \end{bmatrix}\begin{bmatrix} V(x,\omega) \\ I(x,\omega) \end{bmatrix} \tag{1}$$

$Z(\omega)$ and $Y(\omega)$ represent the impedance and admittance per unit length, respectively. By decoupling these differential equations, the solutions describing forward and backward-propagating waves can be expressed as:

$$V(x,\omega) = V^{+}e^{-\gamma(\omega)x} + V^{-}e^{+\gamma(\omega)x} \tag{2}$$

$$I(x,\omega) = I^{+}e^{-\gamma(\omega)x} - I^{-}e^{+\gamma(\omega)x} \tag{3}$$

where + represents the forward wave propagating in the positive x direction, and − corresponds to the backward wave. Additionally, $\gamma(\omega)$ denotes the cable propagation constant. The waves generated by PD propagate in both directions toward the cable ends. Along this path, these waves are influenced by the cable's propagation constant, $\gamma(\omega)$, which is defined as:

$$\gamma(\omega) = \alpha(\omega) + j\beta(\omega) \tag{4}$$

in which $\alpha(\omega)$ and $\beta(\omega)$ are the frequency-dependent real and imaginary components of the propagation constant, representing the attenuation and phase constants, respectively [16].

The interaction between these parameters and the PD pulse as it propagates through the cable is more effectively analyzed in the frequency domain, where the analysis is fundamentally based on the TF of all components along the PD path. Hence, the PD signal measured at the detection point in the frequency domain, $P_m(\omega L)$, can be described as follows [26]:

$$P_m(\omega L) = H_{cable}(\omega L)\, H_S(\omega)\, H_F(\omega)\, S(\omega) \tag{5}$$

where $H_{cable}(\omega L)$, $H_S(\omega)$, $H_F(\omega)$, and $S(\omega)$ are the TF of the cable segment in the PD path, sensor, filter, and the frequency spectrum of PD at its source, respectively. Also, the cable TF can be expressed as follows:

$$H_{cable}(\omega L) = \frac{V_{out}}{V_{in}} = e^{-\gamma(\omega)L} = e^{-(\alpha(\omega)+j\beta(\omega))L} \tag{6}$$

The magnitude of $H_{cable}(\omega L)$ can be obtained as below:

$$|H_{cable}(\omega L)| = |e^{-\alpha(\omega)}|.|e^{-j\beta(\omega)L}| = |e^{-\alpha(\omega)}| \tag{7}$$

here, the magnitude of the constant phase is unity, which means that the magnitude of the cable's TF depends only on the attenuation constant. The phase constant, on the other hand, affects the pulse time delay. These conclusions can be expressed as follows [25]:

$$\alpha(\omega) = -\frac{1}{L}\ln|H_{cable}(\omega L)| \tag{8}$$

$$\beta(\omega) = -\frac{1}{L}\angle H_{cable}(\omega L). \tag{9}$$

2.2. Cable-specific attenuation characteristic

Based on Eq. (8), this part establishes a relation between the incident and reflection pulses generated by a single discharge in a cable. This relation forms the basis for an online monitoring system, enabling the localization framework to autonomously identify the relevant incident and reflection pulses, even under challenging conditions such as multi-path propagation, impulse noise, and simultaneous PD events.

Assuming a PD occurs at the point shown in Fig. 2, the incident pulse will travel a distance of d to reach the measurement point, while the reflection pulse will travel a distance of $2L_c - d$. Due to this fact and Eqs. (5) and (6), the ratio between the incident pulse, $P_{mpd}(\omega)$, and the reflected pulse, $P_{rpd}(\omega)$, can be derived as follows:

$$\frac{P_{mpd}(\omega)}{P_{rpd}(\omega)} = \frac{H_{cable}(\omega d)}{H_{cable}(\omega(2L_c - d))} = e^{2(\alpha(\omega)+j\beta(\omega))(L_c-d)} \tag{10}$$

$$\ln\left|\frac{P_{mpd}(\omega)}{P_{rpd}(\omega)}\right| = 2\alpha(\omega)(L_c - d). \tag{11}$$

From the equation presented above, it can be concluded that the magnitude ratio between the incident and reflected pulses is directly proportional to the attenuation constant and the distance between the PD source location within the cable length. Considering the depicted cable in Fig. 3 (for clarity a two-layer cable is illustrated here; however, the analysis applies to all typical shielded cables that can be modeled as shown in Fig. 1), with the given parameters, the cable's attenuation constant can be derived using the following approach:

$$\gamma = \alpha + j\beta = \sqrt{(R' + j\omega L')(G' + j\omega C')} \tag{12}$$

where R', L', G', and C' represent the resistance, inductance, conductance, and capacitance per unit length of the cable, respectively, and can be expressed as follows [31]:

$$R' \approx \frac{1}{2\pi\sqrt{2/\omega\mu_0}}\left[\frac{1}{r_{ic}\sqrt{\sigma_{ic}}} + \frac{1}{r_{oc}\sqrt{\sigma_{oc}}}\right] \tag{13}$$

$$L' \approx \frac{\mu_d}{2\pi}\ln\left(\frac{r_{oc}}{r_{ic}}\right) \tag{14}$$

$$G' \approx \frac{2\pi\sigma_d}{\ln(r_{oc}/r_{ic})} \tag{15}$$

$$C' \approx \frac{2\pi\epsilon_0\epsilon_d}{\ln(r_{oc}/r_{ic})} \tag{16}$$

By substituting (13) to (16) in (12), α can be derived as follows [32]:

$$\alpha \approx \frac{\xi}{2\sqrt{2}}\sqrt{\frac{C'}{L'}}\sqrt{\omega} \tag{17}$$

where:

$$\xi = \frac{1}{2\pi r_{ic}}\sqrt{\frac{\mu_{ic}}{\sigma_{ic}}} + \frac{1}{2\pi r_{oc}}\sqrt{\frac{\mu_{oc}}{\sigma_{oc}}} \tag{18}$$

By simplifying (11) using the detailed calculation of α, the equation can be simplified as follows:

$$\left|\frac{P_{mpd}(\omega)}{P_{rpd}(\omega)}\right| \propto \lambda'.\sqrt{(f)}.(L_c - d). \tag{19}$$

Above equation reveals that the relation between the magnitudes of the incident and reflection pulses within the cable is affected by the cable's physical and electrical parameters (λ'), the frequency of the PD at its origin, and the location of the PD along the cable. This insight provides a foundation for deriving a cable-specific characteristic, which can serve as a tool for accurately identifying the corresponding incident and reflection pulses.

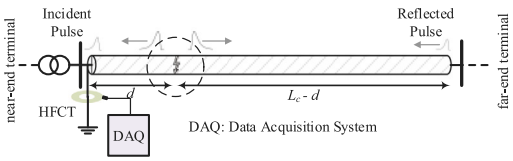

Fig. 2. Schematic representation of the investigated system.

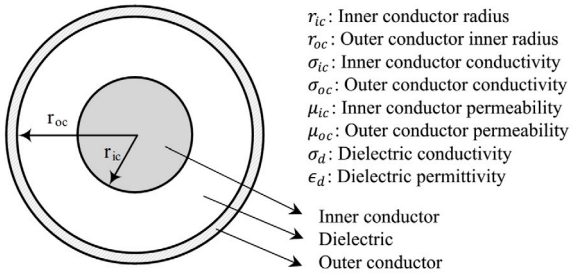

Fig. 3. Geometric characteristics of a power cable.

2.3. Analysis of cable-specific attenuation characteristic

In order to conduct an analysis of the impact of α on the peak ratio of incident and reflected PD pulses, a series of PD events with varying frequencies are applied at 200 m intervals along a 3 km cable with $r_{ic} = 2.2$ cm, $r_{oc} = 3.95$ cm, $\sigma_{ic} = 6 \times 10^7$, $\sigma_{oc} = 4.5 \times 10^6$, $\sigma_d = 10^{-8}$, $\epsilon_d = 4.1$, and $\mu = 1$ for all layers (as shown in Fig. 3). Fig. 4 depicts the achieved outcome.

According to Fig. 4, it is clear that PD pulses characterized by higher frequencies undergo faster attenuation compared to pulses with lower frequencies. This effect is further amplified when there is a significant difference in the distances traveled by the incident and reflected pulses to reach the measurement point. However, once the distance exceeds 1 km from the near-end terminal, the peak ratios of different frequencies start to converge. This convergence can be attributed to the phenomenon where higher-frequency components of the pulses experience stronger attenuation and filtration as they propagate through the longer path, while lower-frequency components are comparatively preserved. Hence, when the location of the PD source moves away from the measurement point, PD pulses with distinct features and frequencies ultimately reach almost the same frequency components, indicating nearly equal peak ratios [25]. Therefore, a corresponding diagram can be generated for each cable, enabling the reliable identification of incident and reflected pulses in measured signals that may contain multiple PD events or impulse noise simultaneously.

The corresponding attenuation characteristic varies because of the difference in the transfer function of different power cables. To generate the diagram shown in Fig. 4, laboratory experiments must be conducted on the relevant power cable sample, or accurate cable parameters should be utilized in simulation-based analyses to derive the cable transfer function, $H_{cable}(\omega L)$. This method facilitates the derivation of the desired attenuation diagram through either experimental or theoretical analysis, offering greater flexibility. Additionally, it is worth noting that the TFs of other components in the PD signal path can be obtained using the same approach.

3. Methodology

This section is organized into three parts. First, the two-step signal segmentation approach is introduced, detailing how the relevant incident and reflection pulses are extracted using the cable-specific attenuation characteristic developed in Section 2. Next, the application of U-Net for precise time estimation is explained. Finally, the complete localization algorithm, integrating these components, is described in detail.

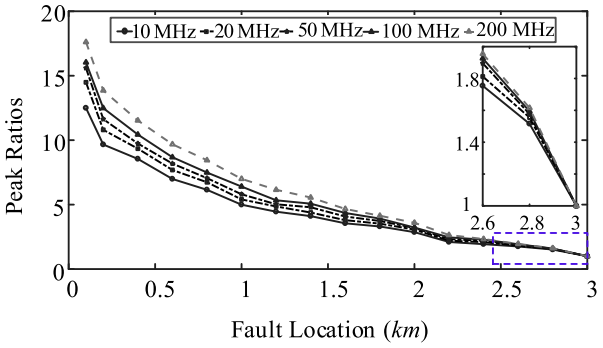

Fig. 4. Ratio of peaks between incident and reflection pulses.

3.1. Two-level signal segmentation

3.1.1. Correlation-based signal partitioning

In online monitoring systems, the signals measured by the sensors are processed by the data acquisition system and then transmitted to the data analysis center. Fig. 5a presents an exemplary signal sample that requires analysis to detect the presence of PD and identify the location of the PD source if detected. As can be seen in Fig. 5a, multiple segments exhibit characteristics resembling a PD pulse. Nevertheless, such segments may originate from multi-path propagation, distinct sources of PD activity at the same time, or may be caused by the presence of impulse noise. Consequently, it is possible to identify and separate all signal segments that exhibit patterns similar to PD pulses. In this context, the signal segments are categorized into those that may contain PD pulses and normal segments that do not contain PD pulses.

In order to specify the signal segments' status, a double-exponential window is utilized for calculating the correlation between each frame of the signal and the moving window. The formulation for this approach is presented below:

$$\rho(j) = \frac{1}{n} \sum_{j=0}^{m} \sum_{i=0}^{n} s(i - kj) r(i) \tag{20}$$

where $\rho(j)$ denotes the correlation output, r and s represent the double exponential window and the signal, respectively. Also, n, k, and m are the window length, window step, and total number of segments in the signal, respectively.

The double-exponential window is particularly effective in PD signal processing, as it amplifies the key features of pulses that exhibit PD-like characteristics in the output. Simultaneously, it effectively filters out periodic noise that might be misinterpreted as PD activity. For example, Fig. 5b presents the correlation calculation result for the signal shown in Fig. 5a. Pulses resembling PD are represented as peaks in the correlation output. Notably, the noise within the time range of 35 to 40 μS is effectively filtered out in the correlation result due to its high-frequency alternating nature. Finally, Fig. 5c illustrates the partitioned signal, divided into four segments that may contain PD pulses. The incident and reflected pulses are present among these segments and require identification. The cable-specific attenuation characteristic developed in Section 2 will be employed to identify the relevant pulses within these segments.

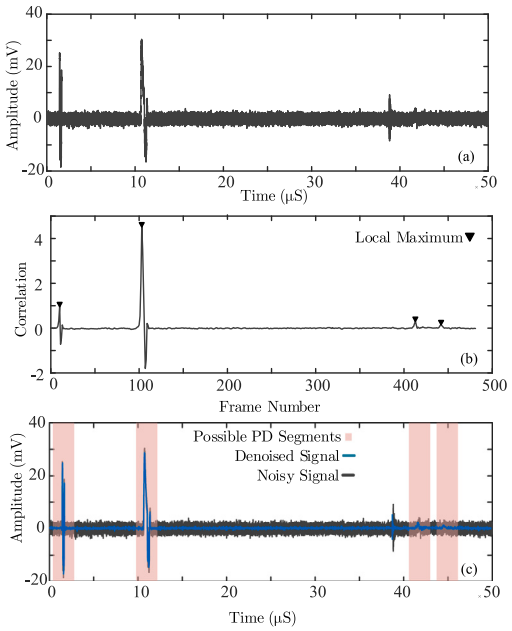

Fig. 5. Signal partitioning procedure (a) a transferred PD sample to the data analysis center, (b) its correlation result, and (c) partitioned output.

3.1.2. Incident and reflected PD pulses identification

The cable-specific attenuation characteristic diagram presented in Fig. 4 can be further improved by including a broader frequency range. Additionally, applying an exponential curve-fitting technique to define upper and lower thresholds for the peak ratio curves ensures that the ratio between incident and reflected pulses lies within the defined range for PDs with varying characteristics. Consequently, after signal partitioning in the first step, the developed cable's attenuation characteristic is utilized to distinguish the incident and reflected segments among the chosen set of segments. In order to accomplish this, an initial estimation of the time difference between the pulses within the segments (Δt_{ij}), as shown in Fig. 6a, must be computed. This estimation procedure is performed using Algorithm 1. In addition to the time difference, the peak ratio of pulses within the segments (R_{ij}) should also be determined. Subsequently, by acquiring the (Δt_{ij}, R_{ij}) pair, it can be positioned accurately on the attenuation characteristic, as shown in Fig. 6b. The determination of segments as incident and reflected can be achieved by analyzing the related pair position with respect to the boundary region of the attenuation characteristic. The presence of pairs within the region of the attenuation characteristic indicates that the corresponding segments are associated with the incident and reflected pulses.

In some scenarios, it is possible for the results obtained from different pairs to fall within the attenuation characteristic curve. This occurrence can often be attributed to the presence of simultaneous PD events or impulse noises, which may have been mistakenly identified as potential PD segments during the signal segmentation process. The ability to distinguish between an actual PD pair and a noise pair relies on the correlation between the statistical features associated with the incident pulse and its corresponding reflection pulse. To achieve this, a set of statistical features, such as peak ratios, time difference (Δt), rising time ratios (t_{rr}), falling time ratios (t_{fr}), full width at half maximum ratios (T_{fwhmr}), area ratios, kurtosis ratios, and skewness ratios are first extracted from each pair. These features are then input into a fully-connected network (FCN), the architecture of which is detailed in Table 1. The FCN produces a binary output, which classifies each pair accordingly. It is worth emphasizing that, due to the relatively straightforward nature of this classification task, a simple FCN architecture is entirely sufficient to achieve effective and reliable results.

Table 1
The details of the employed FCN.

Layer	Output shape	Number of parameters
Flatten	(None, 10)	0
Dense	(None, 128)	1408
Dropout	(None, 128)	0
Dense 1	(None, 64)	8256
Dropout 1	(None, 64)	0
Dense 2	(None, 32)	2080
Dense	(None, 1)	33
Total parameters: 11,777		
Trainable parameters: 11,777		
Non-trainable parameters: 0		

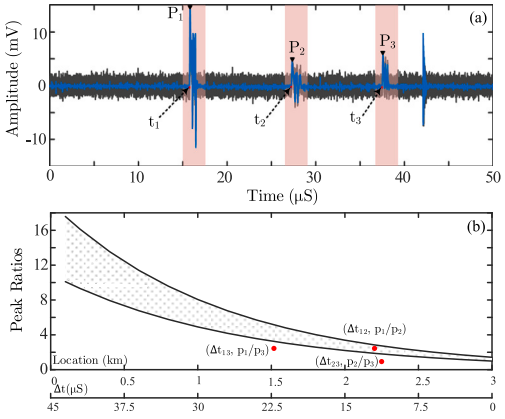

Fig. 6. Collaboration of PD localization components: (a) partitioned signal, (b) incident and reflection pulses determination using cable attenuation characteristic.

Algorithm 1 Time difference estimation algorithm

Input: signal S, suspicious segments $[r_1, r_2, ..., r_n]$ indices
Output: time difference Δt_{ij} array
Initialization :
avg = the average of $|S|$ after removing $[r_1, r_2, ..., r_n]$
for $i = 1$ to n **do**
  t_p= peak position($S[r_i]$)
  j = t_p
  while ($S[j] > avg$) **do**
    j = j-1
  end while
  t[i] = j
end for
for $i = 1$ to $n - 1$ **do**
  for $j = i$ to n **do**
    Δt_{ij} = t[j] - t[i]
  end for
end for
return Δt_{ij}

3.2. Improved arrival time recognition

The integration of the two preceding components identifies the incident and reflected PD segments. However, accurately determining the PD location requires precise calculation of the time difference between these pulses. This is achieved by pinpointing the exact positions of the incident and reflected pulses within their respective segments, thereby facilitating the determination of their arrival times. To address this requirement, the U-Net model is introduced to accomplish this task effectively. The network structure of the U-Net is provided in Table 2.

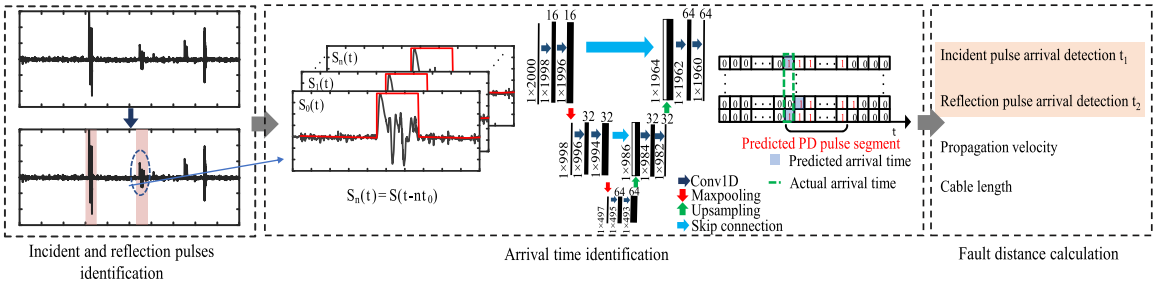

Fig. 7. The procedure for accurate arrival time detection using deep learning.

Table 2
The structure of U-Net for arrival time estimation.

	Layer	Configuration	Output size
Encoder	1: Convolution	Channels: 16, kernel size:3, stride:1	2000
	2: Convolution	Channels: 16, kernel size:3, stride:1	2000
	3: Maxpooling	pooling size:2	1000
	4: Convolution	Channels: 32, kernel size:3, stride:1	1000
	5: Convolution	Channels: 32, kernel size:3, stride:1	1000
	6: Maxpooling	pooling size:2	500
	7: Convolution	Channels: 64, kernel size:3, stride:1	500
	8: Convolution	Channels: 64, kernel size:3, stride:1	500
Decoder	9: Upsampling	–	1000
	Skip connection	Concatenate [5, 9]	1000
	10: Convolution	Channels: 32, kernel size:3, stride:1	1000
	11: Convolution	Channels: 32, kernel size:3, stride:1	1000
	12: Upsampling	–	2000
	Skip connection	Concatenate [2, 12]	2000
	13: Convolution	Channels: 16, kernel size:3, stride:1	2000
	14: Convolution	Channels: 16, kernel size:3, stride:1	2000
	15: Convolution	Channels: 1, kernel size:3, stride:1	2000

The U-Net architecture is widely recognized for its efficacy in segmentation tasks, aligning with the pulse segmentation objective of this study. The input segment, with a fixed length of 2000, undergoes the initial encoding phase in which convolutional layers learn to extract relevant features from the input signal. Simultaneously, pooling layers are employed to downsample the feature maps, reducing spatial dimensions while expanding the receptive field. Subsequently, the decoder part of the network restores the spatial resolution of the feature maps and generates pixel-wise segmentation maps. This is accomplished through the utilization of upsampling layers that increase spatial dimensions, allowing the network to produce segmentations with the same resolution as the input signal. Furthermore, the inclusion of skip connections establishes connections between corresponding encoder and decoder layers and facilitates the preservation of fine details and local contextual information. Consequently, this process enables the identification of the pulse segment within the provided input.

To enhance the performance of the U-Net architecture, it will be fed by N normalized segments, derived from each individual segment, as the input for the model. In simpler terms, by shifting the original segment, N individual segments will be generated. These N segments will serve as input to the U-Net model. Ideally, N sets of outputs should be identical since they are derived from the same segment, as shown in Fig. 7. Nevertheless, due to potential errors, certain outputs may not precisely match the majority. To minimize such errors, the final recognized pulse segment is determined by selecting the result that occurs most frequently. Additionally, enhancing the accuracy of the localization process can be achieved by generating a larger set of shifted samples from each original signal. To optimize this approach, an analysis of the batch size for the U-Net input was conducted. Fig. 8 presents the results of this analysis, demonstrating that generating 10 samples from each signal for the U-Net input yields the lowest deviation from the actual value.

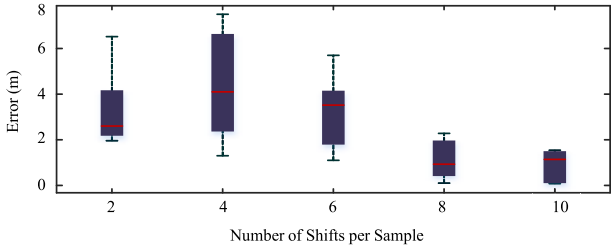

Fig. 8. Impact of number of shifts on the localization accuracy.

3.3. Fault distance calculation

To calculate the fault location, the following equation can be utilized:

$$d = L_c - v\frac{t_2 - t_1}{2} \tag{21}$$

where, L_c represents the total length of the cable, v denotes the propagation velocity of the signal in the cable, and $(t_2 - t_1)$ is the time difference between the incident pulse and the reflected pulse. It is important to note that the propagation velocity v is inherently dependent on the frequency of the discharge event. However, for frequencies exceeding 1 MHz, the propagation velocity exhibits minimal variation and can be considered approximately constant [33]. In this study, an average propagation velocity is calculated for each test system under different frequency conditions, and this averaged value is used as the propagation velocity in the fault location calculations. Finally, the flowchart of the proposed algorithm is provided in Fig. 9 to illustrate the step-by-step process of the proposed method.

4. Results and discussion

4.1. Establishment of the test model

A system similar to Fig. 10a has been implemented in PSCAD/EMTDC to evaluate the performance of the proposed method. As illustrated, to simulate the impedance of other equipment under operational conditions, 50-ohm resistors were connected at both ends of the cable, and also an HFCT sensor, with a bandwidth ranging from 80 kHz to 100 MHz, was placed at one end of the cable. The system operated at a sampling rate of 1 GHz, corresponding to a sampling interval of 1 ns. Additionally, a reduced sampling rate of 200 MHz (5 ns interval) was tested to assess its impact on the results. PD events were simulated using a double exponential model as a PD simulator. The measured data underwent an augmentation process and were subjected to various types of noise, including white noise, modeled as a zero-mean Gaussian with a standard deviation of 5 mV, periodic noise, with frequencies ranging from 1 to 5 MHz and amplitudes between 1 and 10 mV, and impulse noise, with amplitudes set between 1 and 20 mV.

The SNRs of the synthetic PD signals can be adjusted during the augmentation process based on their energy levels. Also, to mitigate

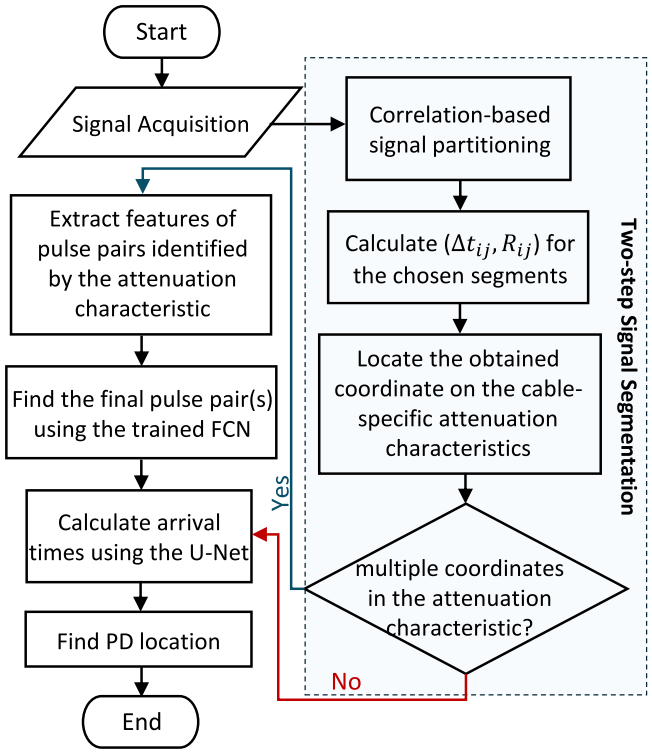

Fig. 9. Proposed localization flowchart.

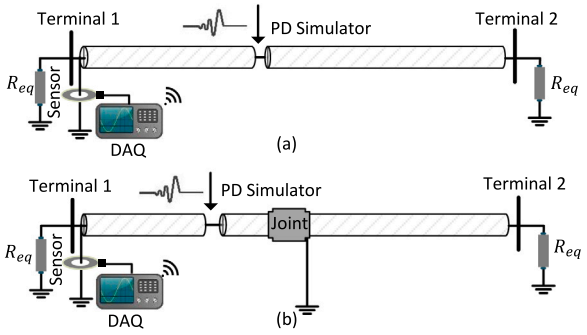

Fig. 10. The test setup of the proposed localization method. (a) Case A test setup, (b) Case B test setup.

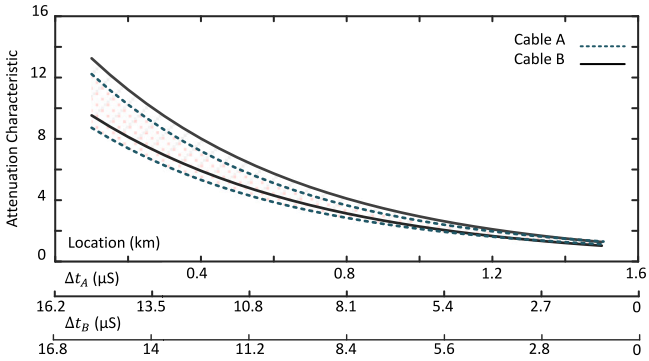

Fig. 11. The attenuation characteristics for Case A and Case B cables.

the risk of data leakage and enhance the U-Net model's generalization capability for unseen samples, two independent datasets were generated: one for training and the other for testing purposes. These datasets were generated using separate cables with different parameters. Table 3 provides detailed information about the cables used to generate the training and test datasets, specifics about the training and test datasets, and the HFCT model. Additionally, to account for the progression of PD activity from its initiation, the synthetic PD signals were categorized into three severity levels based on charge magnitude: mild ($q < 300$ pC), mid-level ($300 < q < 500$ pC), and severe ($q > 500$ pC) [34]. Finally, based on the test model establishment detailed here, two scenarios were designed to evaluate the performance of the proposed method, as outlined below:

- **Case A**: To evaluate the performance of the proposed method under various conditions, including scenarios involving multiple PD-like pulses and concurrent PD events within the system, a homogeneous XLPE cable (Cable 2 in Table 3) with a length of 1.5 km is used as the test case. Additionally, this study considers two distinct SNR levels, 0 dB and −3 dB, to assess the method's performance in noisy environments.
- **Case B**: To evaluate the performance of the proposed method under multipath conditions, an inhomogeneous cable system, consisting of two 0.75 km XLPE cables (Cables 3 and 4 in Table 3) is considered in this study. This setup is designed to simulate realistic scenarios where signal reflections and distortions due to cable joints and inhomogeneities are present. Furthermore, the performance of the proposed method is investigated under a reduced sampling rate, and the results are compared with those obtained using the original sampling rate. This analysis evaluates the method's effectiveness when operating with lower-resolution data, which is critical for practical applications where high sampling rates may not always be feasible.

It is important to highlight that, to improve the accuracy of fault localization, a wavelet-based denoising technique (BayesShrink method using symlet 8 wavelet) at a relatively high decomposition level of 8 was employed. This approach effectively reduces noise while preserving the essential features of the signal, thereby enhancing the localization accuracy. Finally, the attenuation characteristics for each test cable configuration are presented in Fig. 11.

Table 3
Employed training and test cables and dataset parameters.

Set type	Training	Test		
Parameters	Cable 1	Cable 2	Cable 3	Cable 4
r_{ic} (cm)	2.2	2.2	1.8	2.3
r_{oc} (cm)	3.95	3.95	3.6	4.17
σ_{ic} (S/m)	6.93×10^7	5.54×10^7	5.81×10^7	6.93×10^7
σ_{oc} (S/m)	4.98×10^6	3.6×10^6	4.26×10^6	5.5×10^6
μ_{ic}	1	1	1	1
μ_{oc}	1	1	1	1
ϵ_d	3.2	3.84	3.7	3
Datasets detail				
	Training & Validation	Test		
Dataset size	10 920	3280		
PD vs. Noise	45%, 55%	50%, 50%		
Cable type	XLPE	XLPE		
Defect type	Internal	Internal		
Cable length	3 km	Variable		
HFCT model				
$F(s) = \frac{-0.00051s}{6\times10^{-12}s^2+0.000142s+10}$				

4.2. Performance evaluation under case A conditions

In this study, PD signals were randomly extracted from the test dataset to replicate real-world measurement conditions over a time span of 50 μS, with a predefined measurement interval. The signals were sampled from PD events occurring at intervals of 200 m along the

cable. During the testing phase, the average propagation velocity of the signals was measured at 1.74×10^8 m/S, and this value was employed for the subsequent localization calculations. To thoroughly assess the segmentation capability of the proposed method, both impulse noise and periodic noise were intentionally amplified. Furthermore, multiple simultaneous PD events were simulated to evaluate the method's robustness under this scenario. These tests were conducted under two distinct SNR levels of 0 and −3 dB. The localization results obtained from these experiments are detailed in Table 4.

To further explore the process, several samples used during the testing phase are provided here for deeper analysis. Fig. 12 illustrates a sample containing multiple segments resembling PD pulses, which could represent actual PD pulses, impulse noise, switching transients, or other system interferences. Such scenarios in real-time operations pose significant challenges for monitoring systems based on single-end measurement schemes, as they must accurately identify relevant incident and reflection pulses within the measurement to perform the localization task effectively. The localization process begins with the calculation of correlation for each window of the measured signal to isolate segments that may contain PD pulses. In the subsequent step, based on the peak ratio and the time difference between potential PD pulses within each segment, the coordinates $(\Delta t_{ij}, \frac{p_i}{p_j})$ are determined. These coordinates are then compared against the cable's attenuation characteristics to verify whether they fall within the defined range for relevant incident and reflection pulses. This process narrows down the possible PD segments, which can initially form numerous combinations of pairs, to ultimately identify the correct incident and reflection pulse pair. For the example shown in Fig. 12a, six pulses are present in the measurement. During the initial signal segmentation using correlation, four segments with potential PD pulses were selected (highlighted in red), while two segments, due to their highly periodic nature, were excluded from the final correlation curve (highlighted in green). From the set of four segments, six possible pairs can be formed, each of which could potentially be the final incident and reflection pulse pair.

The coordinates $(\Delta t_{ij}, \frac{p_i}{p_j})$ for each of these pairs are calculated and presented in Table 5. The relative position of these pairs with respect to the attenuation curve, as shown in Fig. 12b, helps identify the correct incident and reflection pulses. In this example, based on the obtained information from Table 5 and the results shown in Fig. 12b, among the detected pulses, two potential incident-reflection pairs are identified, one comprising the first and third pulses and the other involving the first and second pulses. The presence of these pairs within the attenuation characteristic indicates two possible scenarios. Either multiple PD events have occurred simultaneously, or one of the pairs is the result of an interference pulse resembling PD-like behavior. To resolve this uncertainty, the trained FCN is used to analyze the statistical features of each pair. Based on this assessment, the FCN classifies the first and third pulses as the actual PD pair, while the other pair is classified as a non-PD event. Once the relevant incident and reflection pulses are identified, the U-Net model is used to precisely determine their time difference. This is achieved by identifying the exact position of each pulse within its segment. The absolute time reference of these pulses within the measured signal are then used to compute the time difference, which is 10.3589 μS. Based on this time difference, the location of the PD defect is estimated to be 598.78 m away from the measurement point.

Also, in cases where multiple PDs occur simultaneously in the cable, several pulse pairs appear within the attenuation characteristic. Fig. 13a presents a measured example containing concurrent PD pulses. Following the same identification process, as shown in Fig. 13b two pulse pairs, one including the first and fourth segments and another including the second and third segments, are recognized as potential incident and reflection pulses. By extracting these pairs' features, as provided in Table 6, and applying the FCN, both pairs are classified as PD pairs, indicating the presence of multiple simultaneous PD sources. Subsequently, using the U-Net, the time difference for the first pair

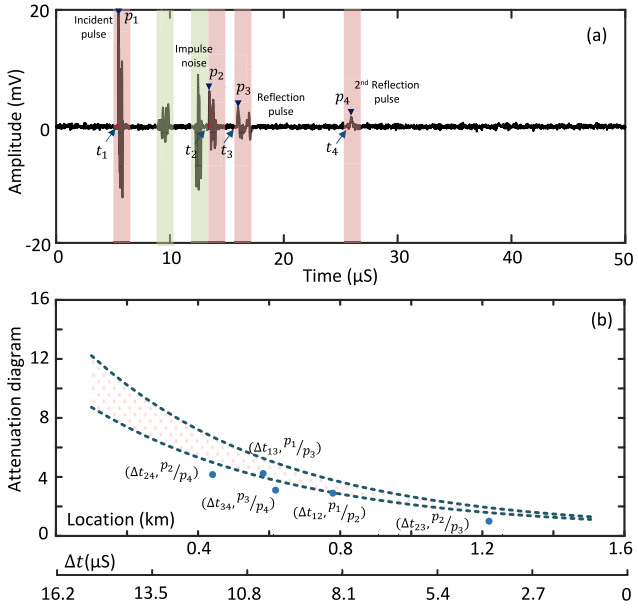

Fig. 12. Homogeneous cable: (a) the identified possible PD segments within the measured signal, (b) incident and reflection pair identification by the attenuation characteristic.

(first and fourth segments) is determined to be 14.94 μS, while the second pair (second and third segments) has a time difference of 5.74 μS. These correspond to PD source locations at 200.15 m and 1000.86 m, respectively.

Furthermore, Fig. 14 presents a sample of the noisy measurements used in this study, with an SNR of −3 dB. After applying wavelet-based denoising and following the same processing steps, the localization algorithm successfully identified the relevant incident and reflected pulses. The U-Net estimated the pulse arrival times with deviations of 112 and 228 points from the actual arrival times, corresponding to delays of 11.2 nS and 22.8 nS, respectively. Consequently, the time difference between these two pulses was determined to be 14.83 μS, leading to an estimated PD location 210.11 m from the measurement point.

4.3. Performance evaluation under Case B conditions

In this study, the performance of the proposed method is evaluated in a more complex cabling system, where two different cables are connected, as illustrated in Fig. 10b. This configuration causes additional reflection pulses from the cable joint and further distorts the pulses generated by PD activity, posing challenges for single-end measurement schemes. Similar to the previous case, measurements were conducted over a period of 50 μS, but this time a reduced sampling frequency of 200 MHz (5 ns sampling interval) is also employed. The average propagation velocity of the signals in this test was obtained 1.68×10^8 m/S, and this value was used for subsequent localization calculations. Faults were applied at intervals of 200 m along the cable, and the SNR level was set to 0 dB. The localization results for this case, under both 1 GHz and 200 MHz sampling frequencies, are provided in Table 7.

The results in Table 7 show that the localization accuracy under both sampling frequencies is nearly comparable. While reducing the sampling frequency can lead to the loss of certain high-resolution details, such as precise arrival times, which may impact any single-ended localization method relying on arrival time estimation, the proposed approach can still achieve satisfactory accuracy as long as the reflection pulse is detectable. Fig. 15 presents a sample signal from this study, where the PD source is located at 600 m, analyzed using two different

Table 4
Localization results for the homogeneous cable.

SNR	Distance	Recognized pulse error			Localization results		
		Incident[a]	Reflection[b]	Δt (μS)	Calculated (m)	Error (m)	Accuracy
	200	−112 pts	−228 pts	14.83	210.11	+10.11	
	400	+17 pts	−218 pts	12.41	420.5	+20.5	
	600	+103 pts	−186 pts	10.63	574.86	−25.14	
−3 dB	800	−62 pts	−523 pts	7.59	840.13	+40.13	95.48%
	1000	+129 pts	−510 pts	5.11	1055.62	+55.62	
	1200	+32 pts	+725 pts	4.14	1139.72	−60.28	
	1400	+250 pts	+318 pts	0.881	1423.35	+23.35	
	200	−15 pts	−17 pts	14.94	200.15	+0.15	
	400	−13 pts	−14 pts	12.64	400.19	+0.19	
	600	+31 pts	+17 pts	10.36	598.78	−1.22	
0 dB	800	+1 pt	−7 pts	8.03	801.33	+1.33	99.90%
	1000	+4 pts	+14 pts	5.74	1000.86	+0.86	
	1200	+1 pt	+9 pts	3.45	1199.27	−0.73	
	1400	−11 pts	+1 pt	1.138	1401.02	+1.02	

[a] The term 'pts' in these columns represents the number of sampling points deviated from the actual arrival time point.
[b] The term 'pts' in these columns represents the number of sampling points deviated from the actual arrival time point.

Table 5
$(\Delta t_{ij}, \frac{p_i}{p_j})$ calculations for the separated segment in the first step.

Segments	1	2	3	4
1	N/A	(2.86, 8.21)	(5.08, 10.23)	(11.3, 20.16)
2	(0.35, 8.21)	N/A	(1.78, 4.05)	(4.16, 11.88)
3	(0.20, 10.23)	(0.56, 4.05)	N/A	(2.93, 9.89)
4	(0.09, 20.16)	(0.24, 11.88)	(0.34, 9.89)	N/A

Table 6
Extracted pairs' features for the signal shown in Fig. 13.

Features	1st pair		2nd pair		Pairs' features	
	Incident	Reflection	Incident	Reflection	1st pair	2nd pair
Peak (mV)	23.54	2.98	8.8	3.01	7.9	2.92
Δt (μs)	–	–	–	–	29.88	22.98
T_r (ns)	28	61	34	73	0.46	0.47
T_f (ns)	101	142	111	167	0.71	0.66
T_{fwhm} (ns)	92	123	98	147	0.75	0.67
$A \times 10^{-9}$	3.11	0.82	2.83	0.73	3.79	3.88
kurtosis	57.63	21.11	45.19	17.23	2.73	2.62
skewness	2.15	9.18	3.83	13.65	0.23	0.28

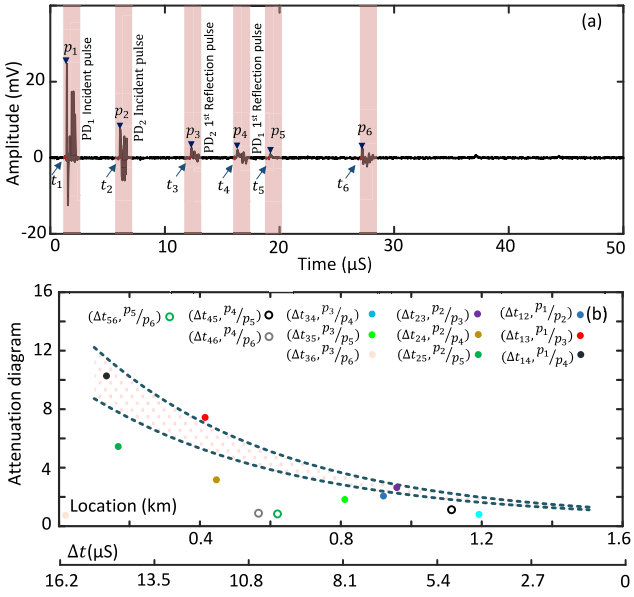

Fig. 13. Homogeneous cable: (a) the identified possible PD segments within the measured signal under multiple PD occurrence, (b) incident and reflection pair identification by the attenuation characteristic.

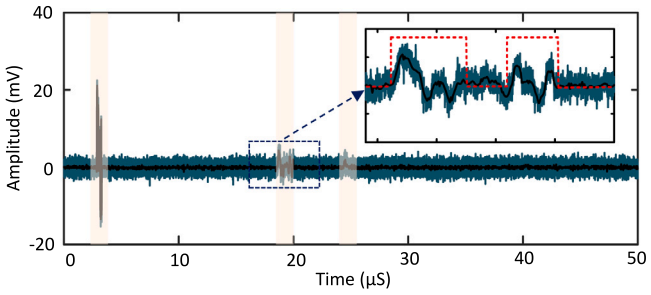

Fig. 14. Signal with a −3 dB SNR: The green line represents the noisy signal, the black line denotes the denoised signal, and the red line illustrates the results obtained using the U-Net model for arrival time detection of the reflection pulse.

sampling frequencies. As shown in Fig. 15a and b, the results for correlation-based calculation and attenuation characteristic are almost the same across both sampling frequencies. This trend was observed for all test samples in this study, indicating that a reduced sampling frequency does not compromise the segmentation process while also significantly expediting the computational process. However, arrival time estimation exhibited some sensitivity to the sampling frequency. As provided in Table 7, when the sampling frequency was reduced to one-fifth of the original value, the accuracy decreased by approximately 2%. To further investigate this effect, Fig. 15c compares the U-Net predictions for the reflection pulse for both 200 MHz and 1 GHz sampling frequencies. At 200 MHz, the U-Net underpredictes the arrival time, resulting in a deviation of +200 ns (+40 points) from the actual value. Conversely, at 1 GHz, the estimated arrival time is slightly delayed, with a deviation of −91 ns (−91 points). These deviations are calculated based on the difference between the actual and estimated arrival times. Using this analysis for the incident pulse and computing the time difference between the incident and the reflection pulses, the estimated PD locations at 200 MHz and 1 GHz are determined to be 628.22 m and 587.28 m, respectively.

Additionally, in this study, the presence of the joint introduces a weak reflection that propagates back toward the cable's head, distorting the reflection pulses and increasing the number of PD-like pulses within the signal. This poses a challenge for online monitoring systems while also altering the cable system's attenuation characteristic due to increased attenuation during PD pulse propagation. As illustrated in Fig. 11, the attenuation curve has been shifted slightly upward, reflecting the impact of multipath propagation on signal attenuation. Despite the challenges introduced during the evaluation, the proposed

Table 7
Localization results for the inhomogeneous cable.

Sampling frequency	Distance	Recognized pulse error			Localization results		
		Incident[a]	Reflection[b]	Δt (μS)	Calculated (m)	Error (m)	Accuracy
200 MHz	200	−14 pts	+13 pts	33.20	211.31	+11.31	96.43%
	400	−30 pts	+11 pts	30.75	417.29	+17.29	
	600	−27 pt	+40 pts	28.34	628.22	+28.22	
	800	−83 pt	+18 pts	26.52	772.44	−72.44	
	1000	−34 pts	+38 pts	23.45	1030.4	+30.4	
	1200	−50 pts	+4 pts	21.66	1180.65	+180.65	
	1400	−88 pts	−14 pts	18.68	1431.02	+31.02	
1 GHz	200	−11 pts	+38 pts	33.28	204.11	4.11	98.49%
	400	−133 pts	−46 pts	30.87	407.28	7.28	
	600	+61 pt	−91 pts	28.72	587.22	−12.78	
	800	−30 pt	+91 pts	26.07	810.13	+10.13	
	1000	−75 pts	+96 pts	23.64	1014.35	+14.35	
	1200	+62 pts	−67 pts	21.56	1189.18	−10.82	
	1400	−1 pts	+160 pts	18.89	1413.5	+13.5	

[a] The term 'pts' in these columns represents the number of sampling points deviated from the actual arrival time point.
[b] The term 'pts' in these columns represents the number of sampling points deviated from the actual arrival time point.

method demonstrated effective and reliable performance in both Case A and Case B. The developed framework effectively handled complex scenarios, including multiple PD-like impulse noises, multiple simultaneous PD events, and multipath propagation, proving its practical suitability for accurate PD localization in online monitoring systems. Additionally, the U-Net architecture achieved high precision in arrival time estimation, further supporting its effectiveness as a component of the approach. In the next part, a detailed comparative analysis is presented, comparing the proposed method with both recent and traditional studies in the field.

4.4. Single-end algorithms comparison

To conduct a meaningful comparison, several key assumptions were established. First, it is assumed that prior knowledge of the relevant incident and reflection pulses is available for the localization algorithm. Additionally, the system is presumed to be free from impulse noise or multiple PD sources that could potentially interfere with the performance of the localization algorithms. The dataset utilized for this analysis was generated under the test conditions of Case A, with the SNR set to 10 dB through data augmentation. Furthermore, the propagation velocity used for location estimation is 1.74×10^8 m/s, which is the average propagation velocity obtained for Case A evaluation. For each location, the estimation process was repeated 10 times, and the average of these calculations was taken as the final result. The error was quantified using the following equation:

$$\delta = \left(\frac{1}{10}\sum_{i=1}^{10}\frac{|d - d_i|}{L}\right) \times 100\% \tag{22}$$

where d is the actual location of the PD defect, d_i is the estimated location, and L is the total length of the cable.

The comparison includes the traditional TDR method, the trigger level method [17], the signal energy method [19], and the proposed method in [10]. Among these, as provided in Table 8, the proposed method and the method described in [10] demonstrate the highest performance. However, it is important to note that while the method in [10] excels in handling variations in propagation velocity and achieves high localization precision under such conditions, it does not address challenges related to impulse noise, multi-path propagation, or the presence of multiple PD sources in the system. Moreover, the identification of reflection pulses within the measured signal is not discussed in [10], which may limit its applicability in real-time, online monitoring systems. This limitation is also present in other TDR-based algorithms. In contrast, the proposed method in this study not only effectively addresses these challenges but also provides high-precision estimation of both incident and reflection pulses, making it a more robust solution for practical applications.

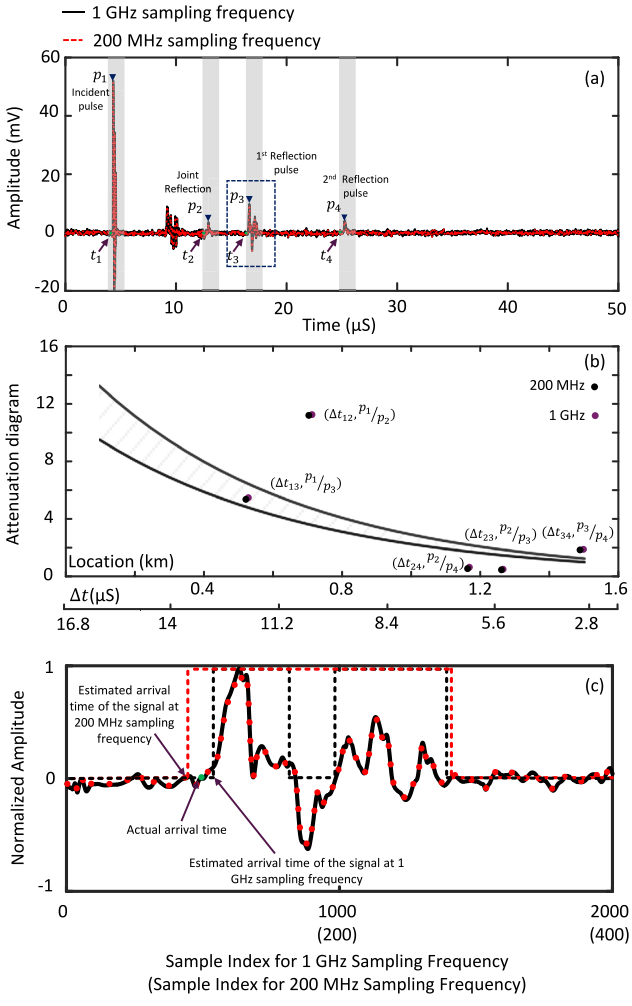

Fig. 15. Inhomogeneous cable: (a) the identified possible PD segments within the measured signal, (b) incident and reflection pair identification by the attenuation characteristic, and (c) detection of the reflection pulse p_3 arrival time using U-Net (the red and black dashed lines represent the U-Net results for signals sampled at 200 MHz and 1 GHz, respectively.).

Table 8
Single-end methods comparison.

Location	TDR		Trigger level		Signal energy		[10]		Proposed	
	d_i	δ%	d_i	δ%	d_i	δ%	d_i	δ%	d_i	δ%
200	194	0.4	187	0.87	201.1	0.07	202.6	0.17	202.1	0.14
400	393	0.47	391	0.6	403.4	0.23	397.9	0.14	401.2	0.08
600	591	0.6	592	0.53	603.4	0.23	600.1	0.007	599.4	0.04
800	788	0.8	791	0.6	809.9	0.66	797.9	0.14	805.7	0.45
1000	982	1.2	988	0.8	1009.3	0.62	995.9	0.27	997.3	0.18
1200	1188	0.8	1183	1.13	1215.7	1.05	1194.1	0.39	1205.1	0.34
1400	1373	1.8	1364	2.4	1434.1	2.27	1410	0.67	1404.8	0.32

Table 9
The maximum performance capability of the proposed method under different conditions.

Freq. (MHz)	SNR = −10 dB		SNR = 0 dB		SNR = 10 dB	
	Noisy	Denoised	Noisy	Denoised	Noisy	Denoised
100	x	x	0.4 km	0.76 km	3.3 km	3.3 km
75	x	x	0.44 km	0.84 km	3.7 km	3.7 km
50	x	x	0.51 km	1.09 km	4.3 km	4.3 km
25	x	x	0.61 km	1.42 km	4.8 km	4.8 km
10	x	x	0.72 km	1.88 km	4.8 km	4.8 km

4.5. Practical implementation considerations and capabilities of the proposed method

The effectiveness of single-end localization techniques depends on the accurate detection of the first reflected pulse, and the proposed method is no exception. However, identifying this reflection presents significant challenges due to various factors. Previous single-end studies have not fully explored these challenges to define the potential and limitations of such approaches. Therefore, a thorough evaluation of the proposed method's capabilities and constraints is essential. This section provides a detailed examination of the key influencing factors.

To accurately localize PD events using the proposed method, a fundamental prerequisite is that the first reflected pulse within the measured signal must be sufficiently discernible to enable its identification as a potential PD segment during the correlation calculation step. This implies that the attenuation and distortion of the reflected pulse must not be so severe as to make it undetectable. Several factors influence the detectability of the reflected pulse, including the background noise level and the efficacy of the denoising algorithm, the incident pulse frequency, the electrical and physical characteristics of the cable, the severity of the PD event, the spatial position of the defect within the insulation, and the cable length.

Considering these factors, the following analysis explores the operational limits of the proposed method focusing on how cable length, noise level, incident pulse frequency, and PD severity impact its performance. The analysis is conducted on the cable configuration described in Case A, with a focus on moderate PD severity levels, defined by discharge magnitudes between 300 pC and 500 pC. This severity range represents a transition from the early stages of insulation degradation to its final breakdown. The results of this investigation are summarized in Table 9.

The results presented in Table 9 demonstrate that at an SNR of −10 dB, where the signal energy is one-tenth of the noise, the identification of reflection pulses is no longer feasible. Consequently, traveling wave-based localization methods struggle to accurately pinpoint PD sources under such severe noise conditions. However, employing a more advanced denoising scheme, capable of preserving critical signal information, could enhance the performance of the proposed method, though this aspect is beyond the scope of this study. On the other hand, when the SNR increases to 0 dB, where the signal and noise energies are equal, the localization accuracy becomes frequency-dependent. In summary, as noise levels decrease, the single-end measurement approach extends its effective coverage, enabling localization over longer cable sections. Nevertheless, it is important to note that the inherent cable attenuation fundamentally limits this extension.

To achieve an online monitoring system, practical implementation aspects must be considered alongside maximum capability and accuracy. One critical factor is the computational burden, which directly impacts the proposed method's real-time realization. The proposed method combines several components for PD localization, with computational tasks that mainly include correlation calculation and DL-based predictions. The correlation calculation for a 50 μs signal with 50,000 sampling points, using a 2000-sample sliding window, requires approximately 2 ms. Additionally, training the U-Net model on 10,000 signals over 100 epochs, with 10 iterations, takes 160 s per epoch on an NVIDIA RTX 3050 GPU. However, once the network is trained, the model is saved, allowing efficient performance, with each prediction taking less than 5 ms. This guarantees that the localization process is optimized for effective real-time implementation.

Furthermore, with the availability of advanced embedded computing boards featuring high-speed processing and data transfer capabilities (in the order of GB/s), coupled with the widespread adoption of cloud computing, the practical implementation of this method is highly suitable for online monitoring systems. In this setup, HFCT measurements are captured using a data acquisition system (DAQ) installed on a local machine. These signals are then transmitted to a centralized server, where the localization algorithm is executed. This architecture not only ensures low-latency, real-time monitoring but also simplifies integration into existing power system infrastructure, making it a viable and efficient solution for continuous assessment and PD localization in cable networks.

5. Conclusion

This paper has presented a novel single-end methodology for PD localization in power cables, combining traveling wave analysis with TF analysis. The proposed approach employs a two-step algorithm that leverages correlation calculations and cable-specific attenuation characteristics, in conjunction with a U-Net model. This combination enables the precise extraction and determination of the arrival times of both incident and reflection pulses. The effectiveness and accuracy of the method were evaluated through two distinct scenarios, each utilizing different cable systems to simulate real-world operating conditions. The results demonstrated that the proposed method is capable of accurately identifying and discriminating relevant incident and reflection pulses, even under challenging conditions such as impulse noise, multi-path propagation, and the presence of other pulses resembling PD signals. These conditions often lead to errors in conventional online localization systems. Furthermore, the results revealed that the proposed method can successfully locate multiple PD pulses occurring simultaneously. Also, through comprehensive testing under relatively low SNR level and reduced sampling frequency, PD source identification with an accuracy of more than 95%, even in the presence of multi-path propagation, multiple PD sources, or impulse noise was achieved. Beyond this, by analyzing the proposed method's maximum capabilities under various conditions, the current study provided valuable insights regarding localization range under different SNR levels, addressing not only the technical performance of the proposed method but also its economic implications for online monitoring systems.

CRediT authorship contribution statement

Morteza Shamsoddini: Writing – original draft, Validation, Methodology, Investigation. **Tongkun Lan:** Writing – review & editing, Supervision. **Seokbum Ko:** Writing – review & editing, Supervision. **Chi Yung Chung:** Project administration.

Declaration of competing interest

The authors declare that they have no known competing financial interests or personal relationships that could have appeared to influence the work reported in this paper.

Acknowledgments

This work was supported by Mitacs through the Mitacs Accelerate program and the International Minerals Innovation Institute (IMII).

Data availability

Data will be made available on request.

References

[1] Antonella Ragusa, Hugh G. Sasse, Alistair Duffy, On-line partial discharge localization in power cables based on electromagnetic time reversal theory-numerical validation, IEEE Trans. Power Deliv. 37 (4) (2021) 2911–2920.
[2] Jinsuo Li, Yunhe Wang, Xiaojing Wang, Jing Yong, Experimental research on incipient fault voltage disturbance model of power cable insulation, Int. J. Electr. Power Energy Syst. 145 (2023) 108687.
[3] Ahmed Thabet Mohamed, Design and Investment of High Voltage Nanodielectrics, IGI Global, 2020.
[4] Ahmed Thabet Mohamed, Emerging Nanotechnology Applications in Electrical Engineering, IGI Global, 2021.
[5] Ahmed Thabet, Mohamed Fouad, Experimental and simulation analysis for insulation deterioration and partial discharge currents in nanocomposites of power cables, Int. J. Electr. Comput. Eng. (2088- 8708) 14 (2) (2024).
[6] Yuxuan Song, Weigen Chen, Fu Wan, Zhixian Zhang, Lin Du, Pinyi Wang, Jian Li, Zhaoguo Wu, Huixian Huang, Online multi-parameter sensing and condition assessment technology for power cables: A review, Electr. Power Syst. Res. 210 (2022) 108140.
[7] Peng Chi, Yuxuan Qin, Yunchun Tao, Rui Liang, Research on condition assessment of XLPE cable based on signal propagation characteristics, Electr. Power Syst. Res. 195 (2021) 107136.
[8] Ahmed Thabet, M. Fouad, Assessment of dielectric strength and partial discharges patterns in nanocomposites insulation of single-core power cables, J. Adv. Dielectr. 11 (04) (2021) 2150022.
[9] Hyeong Min Lee, Geon Seok Lee, Gu-Young Kwon, Su Sik Bang, Yong-June Shin, Industrial applications of cable diagnostics and monitoring cables via time–frequency domain reflectometry, IEEE Sens. J. 21 (2) (2020) 1082–1091.
[10] Rui Liang, Zhe Zhang, Hailong Li, Peng Chi, Guoxin Li, Yunchun Tao, Partial discharge location of power cables based on an improved single-terminal method, Electr. Power Syst. Res. 193 (2021) 107013.
[11] Hobin Lim, Gu-Young Kwon, Yong-June Shin, Fault detection and localization of shielded cable via optimal detection of time–frequency-domain reflectometry, IEEE Trans. Instrum. Meas. 70 (2021) 1–10.
[12] Junbai Chen, Yuan Yan, Kun Zhao, Mengxin Zhu, Li Wang, Yuxin Lu, Zhe Hou, Hongjie Li, Improved double-sided partial discharge location method for high-voltage cables via pulse-injected time synchronization and variational mode decomposition, IEEE Trans. Instrum. Meas. (2024).
[13] Saike Yang, Xianhai Pang, Peng Zhang, Hongjie Li, Yuan Yan, Junbai Chen, A distributed PD detection method for high voltage cables based on high precision clock synchronization, Measurement 241 (2025) 115731.
[14] Weiqi Qin, Guoming Ma, Sihan Wang, Jing Hu, Tengjun Guo, Rong-Bin Shi, Distributed discharge detection based on improved COTDR method with dual frequency pulses, IEEE Trans. Instrum. Meas. 72 (2023) 1–8.
[15] Yuxuan Song, Haoyuan Tian, Zongqing Jia, Weigen Chen, Weikai Zhang, Changding Wang, Tao Zhou, Litong Li, Deng Hong, Yan Wang, et al., Distributed partial discharge acoustic signal detection and localization technology for GIL with built-in fiber optics, J. Lightwave Technol. (2024).
[16] Marko Hudomalj, Andrej Trost, Andrej Čampa, Traveling wave method for event localization and characterization of power transmission lines, Electr. Power Syst. Res. 232 (2024) 110382.
[17] F.H. Kreuger, M.G. Wezelenburg, A.G. Wiemer, W.A. Sonneveld, Partial discharge. xVIII. Errors in the location of partial discharges in high voltage solid dielectric cables, IEEE Electr. Insul. Mag. 9 (6) (1993) 15–22.
[18] J. Granado, A. Torralba, C. Alvarez-Arroyo, Improving partial discharges location under dispersion and multi-path propagation, Int. J. Electr. Power Energy Syst. 127 (2021) 106638.
[19] C. Herold, T. Leibfried, S. Markalous, I. Quint, Algorithms for automated arrival time estimation of partial discharge signals in power cables, in: Proc. Int. Symp. High Volt. Eng., ISH, 2007.
[20] Xie Min, Zhou Kai, Zhao Shilin, He Min, Zhang Fuzhong, Zhao Wei, Improved cross-correlation algorithm for partial discharge location considering frequency-varying characteristics of phase velocity, Power Syst. Technol. 42 (2018) 1661–1667.
[21] Tabi Fouda Bernard Marie, Yang Bin, Han Dezhi, An Bowen, Principle and application state of fully distributed fiber optic vibration detection technology based on Φ-OTDR: A review, IEEE Sens. J. 21 (15) (2021) 16428–16442.
[22] Liang Guo, Zhiqing Nie, Guangfu Liu, A detection method for cable local defects based on born iteration, Electr. Power Syst. Res. 226 (2024) 109956.
[23] J. Granado, A. Torralba, C. Álvarez-Arroyo, Modeling dispersion of partial discharges due to propagation velocity variation in power cables, Electr. Power Syst. Res. 137 (2016) 124–132.
[24] Tomohiro Kawashima, Yoshinobu Murakami, Naohiro Hozumi, Fundamental study on partial discharge measurement in high-voltage cable terminal joint model and waveform reconstruction by deconvolution processing, in: 2024 10th International Conference on Condition Monitoring and Diagnosis, CMD, IEEE, 2024, pp. 669–672.
[25] Bojie Sheng, Chengke Zhou, Donald M Hepburn, Xiang Dong, Graham Peers, Wenjun Zhou, Zeyang Tang, A novel on-line cable pd localisation method based on cable transfer function and detected pd pulse rise-time, IEEE Trans. Dielectr. Electr. Insul. 22 (4) (2015) 2087–2096.
[26] Mahdi Mahdipour, Asghar Akbari, Peter Werle, Hossein Borsi, Partial discharge localization on power cables using on-line transfer function, IEEE Trans. Power Deliv. 34 (4) (2019) 1490–1498.
[27] Bojie Sheng, Chengke Zhou, Donald M Hepburn, Xiang Dong, Graham Peers, Wenjun Zhou, Zeyang Tang, Partial discharge pulse propagation in power cable and partial discharge monitoring system, IEEE Trans. Dielectr. Electr. Insul. 21 (3) (2014) 948–956.
[28] Marco Tozzi, Andrea Cavallini, GC Montanari, GL Giuliattini Burbui, PD detection in extruded power cables: an approximate propagation model, IEEE Trans. Dielectr. Electr. Insul. 15 (3) (2008) 832–840.
[29] Paul Wagenaars, Peter AAF Wouters, Peter CJM Van Der Wielen, EF Steennis, Approximation of transmission line parameters of single-core and three-core XLPE cables, IEEE Trans. Dielectr. Electr. Insul. 17 (1) (2010) 106–115.
[30] Joel Yeo, Huifei Jin, Armando Rodrigo Mor, Chau Yuen, Norasage Pattanadech, Wayes Tushar, Tapan K Saha, Chee Seng Ng, Localisation of partial discharge in power cables through multi-output convolutional recurrent neural network and feature extraction, IEEE Trans. Power Deliv. 38 (1) (2022) 177–188.
[31] S.W. Ellingson, Electromagnetics, Volume 2, in: Online access: Center for Open Education Open Textbook Library, Number v. 2, Virginia Tech Publishing, 2019, URL https://books.google.ca/books?id=A4kayQEACAAJ.
[32] Antonella Ragusa, Hugh Sasse, Alistair Duffy, Farhad Rachidi, Marcos Rubinstein, Electromagnetic time reversal method to locate partial discharges in power networks using 1D TLM modelling, IEEE Lett. Electromagn. Compat. Pr. Appl. 3 (1) (2020) 24–28.
[33] Kai Zhou, Yao Fu, Guangya Zhu, Shilin Zhao, Lu Lu, Xianjin Wang, Yuan Li, Pengfei Meng, Shiyu Ma, Partial discharge localization on power cables based on a novel signal relay system, IEEE Trans. Instrum. Meas. 71 (2022) 1–9.
[34] Ji Man Park, Jeong Chay Jeon, Ga Ram Han, New approach in partial discharge diagnosis and maintenance of 22.9 kV XLPE power cables in service, Electr. Eng. 101 (4) (2019) 1199–1209.